# Metamaterial Absorber for THz Polarimetric Sensing

Wang, Bingnan; Sadeqi, Aydin; Ma, Rui; Wang, Pu; Tsujita, Wataru; Sadamoto, Kota; Sawa, Yoshitsugu; Rezaei Nejad, Hojatollah; Sonkusale, Sameer; Wang, Cheng; Kim, Mina; Han, Ruonan

TR2018-024     February 23, 2018

## Abstract

THz encoders have distinct advantages for position sensing compared with other types of encoders, such as those based on optical and inductive sensors. A polarization-dependent metamaterial absorber reflects one polarization while absorbs the other, which makes it an ideal building block for the barcode of a THz encoder system. In this paper, we present the design, fabrication, and experiments of a THz polarization-dependent metamaterial absorber, and its application to a polarimetric sensing system.

*SPIE Photonics West*

# Metamaterial Absorber for THz Polarimetric Sensing

Bingnan Wang[a], Aydin Sadeqi[c], Rui Ma[a], Pu Wang[a], Wataru Tsujita[b], Kota Sadamoto[b],
Yoshitsugu Sawa[b], Hojatollah Rezaei Nejad[c], Sameer Sonkusale[c], Cheng Wang[d], Mina Kim[d],
and Ruonan Han[d]

[a]Mitsubishi Electric Research Laboratories, 201 Broadway Ste 8, Cambridge, MA 02139 USA
[b]Advanced Technology R&D Center, Mitsubishi Electric Corp. Amagasaki City, 661-8661,
Japan
[c]Nano Lab, Department of Electrical and Computer Engineering, Tufts University, 161 College
Ave. Medford, MA 02155
[d]Department of Electrical Engineering and Computer Science, MIT, Cambridge, MA, 02139

## ABSTRACT

THz encoders have distinct advantages for position sensing compared with other types of encoders, such as those based on optical and inductive sensors. A polarization-dependent metamaterial absorber reflects one polarization while absorbs the other, which makes it an ideal building block for the barcode of a THz encoder system. In this paper, we present the design, fabrication, and experiments of a THz polarization-dependent metamaterial absorber, and its application to a polarimetric sensing system.

## 1. INTRODUCTION

Terahertz (THz) waves have distinct features that make them advantageous in various sensing and imaging applications.[1,2] THz waves can see through most opaque (non-metallic, non-polar) materials, making them suitable for probing concealed objects; the rotational mode and vibrational mode frequencies of most molecules lie in terahertz region and have distinct spectral features, making THz waves suitable for chemical sensing; THz radiation is non-ionizing and non-destructive, and exposes minimal health risk, making it suitable for commercial uses such as security scanning and medical imaging.[3] For industrial applications, THz has long been investigated for quality control using THz time-domain spectroscopy and imaging across various sectors, such as the food production,[4] semiconductor integrated circuit manufacturing,[5] etc.

In this paper, we explore the use of THz waves for linear position sensing based on a polarization-dependent encoder. Linear position sensors detects the position of a linear scale or "barcode" when it has linear movement relative to the sensor head. Position sensing is highly desirable in many industrial applications, such as integrated circuit assembly equipment, laser scanners and printers. There are many existing technologies for linear position sensing, including inductive encoder, magnetic encoder, and optical encoder.[6] Each type of encoder has different characteristics, such as the accuracy, reliability, operating condition, and cost. For optical encoders, foreign matter such as dirt or grease can cause sensor failure with little warning. Magnetic encoders require precision housings and mechanical assembly to avoid errors caused by magnet or sensor misalignment. Inductive encoders have advantages in reliability, cost, and susceptibility to harsh environment; however,due to the relatively large sensor size and low operating frequency, the resolution is often limited. THz sensors have the potential to balance accuracy and reliability and provide a better alternative technology. In terms of reliability, THz based sensing and imaging systems have been demonstrated to work under harsh environment such as smoke and fire,[7,8] making them more reliable than optical and magnetic encoders. On the other hand, compared with inductive sensor based encoders, THz position sensors can achieve better resolution due to the fundamental difference in sensing mechanism and the sub-millimeter wavelength.

Our proposed THz encoder system utilizes the polarization properties of the THz waves, with a sensor generating a polarized signal, and a polarization-dependent barcode. In the following of the paper, we will first introduce the encoder system working principles and how metamaterial absorber is related to the system; next we will move on to the metamaterial absorber design for the sensing system; some initial experiment results will be presented as well.

## 2. THE THZ ENCODER SYSTEM

In the proposed THz encoder, there are two major components in an encoder: the sensor, and the barcode. A block diagram of the system is shown in Fig. 1. A THz transceiver, which is a combination of emitter and receiver, is used as the sensor, and transmits linearly polarized signal through a transmitting antenna to the scale; the polarized signal is reflected from the polarization-dependent barcode, and collected by another receiving antenna. Each received signal is analyzed by the processor, and mapped to a particular position. The barcode is designed such that each pixel responds differently to the linearly polarized incident signal. In general, polarimetric sensing is a method to measure and interpret the polarization of electromagnetic waves in a sensing system. Polarimetry has been widely utilized in microwave and optical regime, such as polarimetric weather radars and other remote sensing systems, and recently proposed for THz imaging systems.[9]
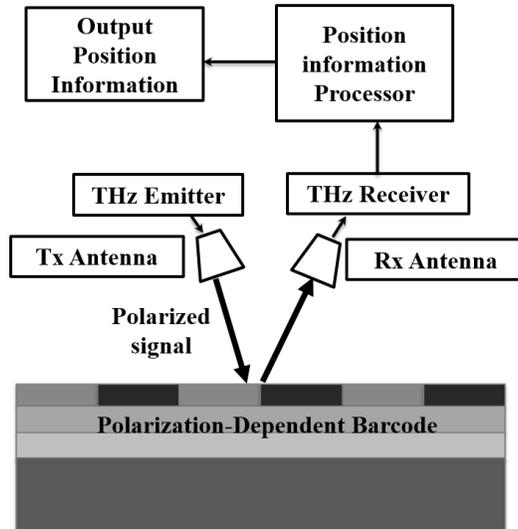


Figure 1. The diagram of proposed THz encoder system.

For the polarization-dependent barcode, one obvious choice is to use polarizers. A simple linear polarizer using wire grating film (WGF) is capable to perfectly reflect one polarization while pass through the other, as shown in Fig. 2(a). For one polarization where the electric field is parallel to the wires, the signal is reflected back; for another polarization where the electric field is perpendicular to the wires, the signal passes through. If additional materials are added to the polarizer, e.g., as substrate, additional reflection can happen to the polarized signal that passes through. Objects behind the WGF polarizer can also result in additional reflections which potentially corrupt the reflected signal. Therefore, there is a need to design a polarizer that is mechanically stable and less susceptible to noises due to reflection from external objects.

A polarization-dependent metamaterial absorber, on the other hand, perfectly reflects one polarization while absorbing the other, with no signal passes through it, as shown in Fig. 2(b). Next, we will show the principle and design of metamaterial absorber for the THz sensing system.

### 2.1 Polarization-Dependent Metamaterial Absorber

A metamaterial absorber is capable of absorb most of the incident wave at designed operating frequencies by using metamaterial structures.[10–12] The original design of metamaterial absorber consists of three-layer metal-dielectric-metal structures, and excites both electric and magnetic resonances at the same frequency band, in order to achieve almost perfect absorption.[10] At each frequency the absorption power $A = 1 - T - R$, where $T$ is the transmitted power and $R$ is the reflected power. For the metamaterial absorber, $R$ is very small, due to the impedance matching condition with the free space, $T$ is also very small, due to the strong absorption and field enhancement at the absorber. As a results, over 90% absorption was observed.[10] Later on, various metamaterial absorber designs and experimental demonstrations across the frequency spectrum have been reported.[11–13]
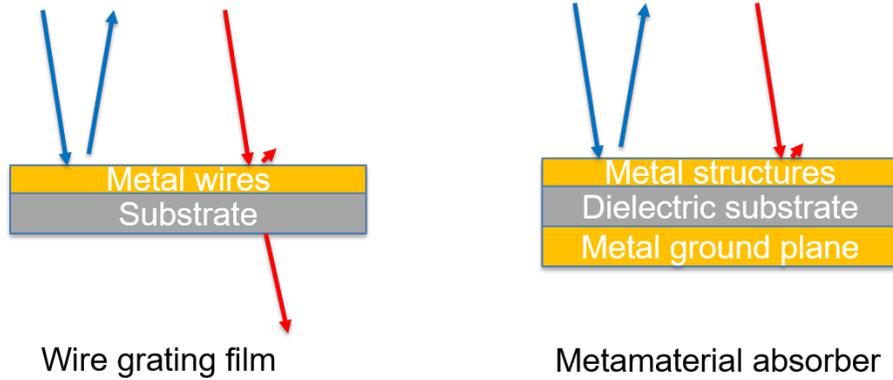
Figure 2. (a) The response of a wire grating film polarizer to two different polarization. (b) The response of a polarization-dependent metamaterial absorber to two different polarizations.

Instead of original design with resonator structures on both sides of the dielectric spacer, a popular configuration is to have a top layer with metal resonator structures and a metal ground plane separated by a dielectric spacer,[13,14] as illustrated in Fig. 2(b). The advantage of this configuration is that transmission is completely eliminated by the ground plane, $T = 0$. The incident wave is either reflected or absorbed. A lot of publications have contributed to the theoretical development of the metamaterial absorbers, either by lumped circuit model,[14,15] or interference theory.[16] In brief, we can contribute the strong absorption to the combination effect of the electrical resonance due to the top metal structures, and the Fabry–Pérot effect due to multi-reflection between the top layer and ground plane. Therefore, both the metallic structure geometry, and the dielectric material properties of the spacer including the loss tangent determine the absorption spectrum.
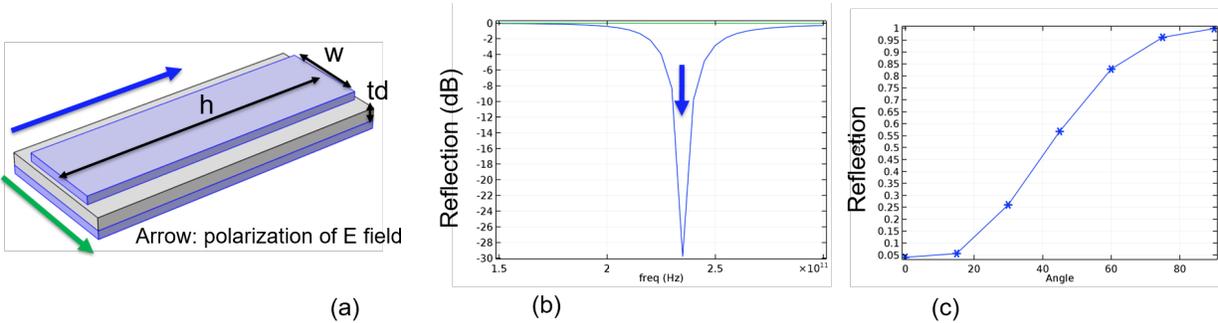


Figure 3. (a) The unit cell structure used for simulation: The top metal (gold) patch has width $w = 120\mu$m and length $h = 340\mu$m, and the unit cell size is $175\mu$m $\times 350\mu$m. The thickness of the dielectric spacer (parylene-C) is $t_d = 17\mu$m. The metal layer thickness is 100 nm. (b)Simulated reflection spectrum with two different polarizations. (c) Reflected power as a function of rotation angle.

While the majority of metamaterial absorbers are trying to achieve polarization-independent absorption, our purpose is to maximize the polarization-dependence of absorption, so that high contrast can be realized for sensing purpose. The unit cell of our metamaterial absorber design is shown in Fig. 3(a), where the top layer is a rectangular shaped patch, with the parameters showed in the caption. The structure is designed to operate at the dipole resonance along the long side of the patch. Both the top layer and ground plane are gold and have thickness of 100 nm. The dielectric spacer is parylene-C, which has been widely used in many areas, such as nanotechnology, electronics, medical, and pharmacopoeia industries, due to its excellent mechanical, physical, electrical, and barrier properties. Industry applications typically use a chemical vapor deposition technique to form a parylene layer, and a wide thicknesses range can be realized. The thin film is also conformal for almost

every exposed surface and is pinhole-free. With these superior features, parylene has been shown to be a good candidate for THz metamaterial substrates.[17]

When the incident wave has the electric field along the long side, the resonance is excited, low reflection and high absorption is expected. The structure is modeled in COMSOL Multiphysics, and the reflection spectrum is plotted for both polarizations in Fig. 3(b). When electric field is polarized along the long side of the patch, a sharp resonance is seen at around 235 GHz, where the reflection drops to -30 dB. While for the other polarization, there is no response at the same frequency range, and all the power is reflected back. We design the metamaterial absorber such that the resonant absorption peak is at the operating frequency of the sensor. The high contrast ratio between two polarizations is important to for the polarimetric sensing system. In Fig. 3(c), we show the reflected power as a function of rotation angle of the electric field, with 0° being in parallel with the long side of the rectangular patch. We can see that the power varies from 0.05 to 1, when the polarization is rotated from 0° to 90°.

With the design parameters in place, we started the fabrication and experiment process.
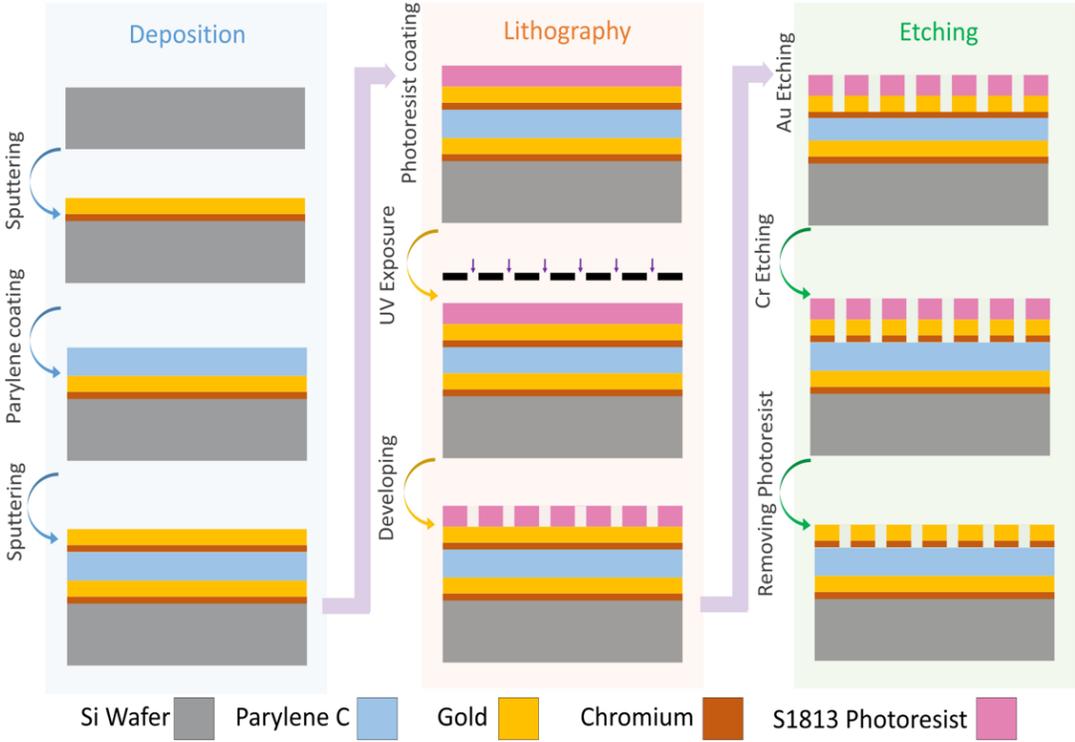
## 3. FABRICATION & EXPERIMENT



Figure 4. The fabrication process flow for THz metamaterial absorber.

The fabrication process flow of the metamaterial absorber is shown in Fig. 4. It starts by cleaning 100 mm N-type silicon wafer using acetone, isopropyl alcohol and distilled water respectively. The wafer was dried with a nitrogen gun and placed on hot plate at 115°C for 2 minutes. NSC-3000 Magnetron Sputter tool was used to deposit 10 nm of chromium followed by 100 nm of gold layers on the wafer; the chromium layer was deposited to increase the adhesion of gold to the substrate. Parylene was coated with desired thickness to serve as the dielectric layer using the PDS2010 Parylene coater (from Specialty Coating Systems™). Parylene surface

was cleaned for 10 seconds by reactive ion etching (RIE) to increase the adhesion. Ten seconds is enough to clean the surface without altering the thickness of parylene layer significantly. Consequently, 10 nm and 100 nm of Chromium and gold were deposited by sputtering tool on the parylene layer. A custom glass mask was designed in house and then ordered from Advance Reproduction Corporation to carry out lithography process. Photoresist (S1813 by Dow®Chemicals) was used for patterning the metamaterial structure. The photoresist was spin-coated at 2000 rpm on the gold layer to achieve the thickness of approximately 2 $\mu$m and later baked for 1 minute in 115°C. Later on, the sample was exposed to UV light for 7 seconds (OAI Model 204IR Mask Aligner, OAI corp.) with the power intensity of 20.04 mW/cm$^2$. The photoresist layer was then developed in MICROPOSIT Developer (Dow®chemicals) for 45 seconds. The developer solution was prepared by diluting MICROPOSIT Developer with distilled water with volume ratio of 2:1 (water:developer). Subsequently, wafer was place in distilled water for 1 minutes to remove the residues of developer. Next, the sample was placed in a petri dish containing gold etchant to etch the gold between the photoresist patterns and then rinsed with distilled water for 1 minute. After that, the sample was placed in chromium etchant to etch away the chromium and was rinsed with distilled water for 1 minute. The gold etchant type TFA and chromium etchant 1020 was supplied by TRANSENE Company, Incorporated. The amount of time for etching the chromium and gold is variable depending on the etch rate of the etchants but in order to get uniform etching with less variations we mixed the etchant with water with a ratio of 1:1 (water to etchant). Eventually, the wafer was rinsed with acetone to remove the photoresist on the top layer then rinsed with Isopropyl alcohol and water, each for 1 minute. Finally, to clean the surface from any remaining residue, the device was placed in RIE machine and treated with oxygen plasma for 1 minute.
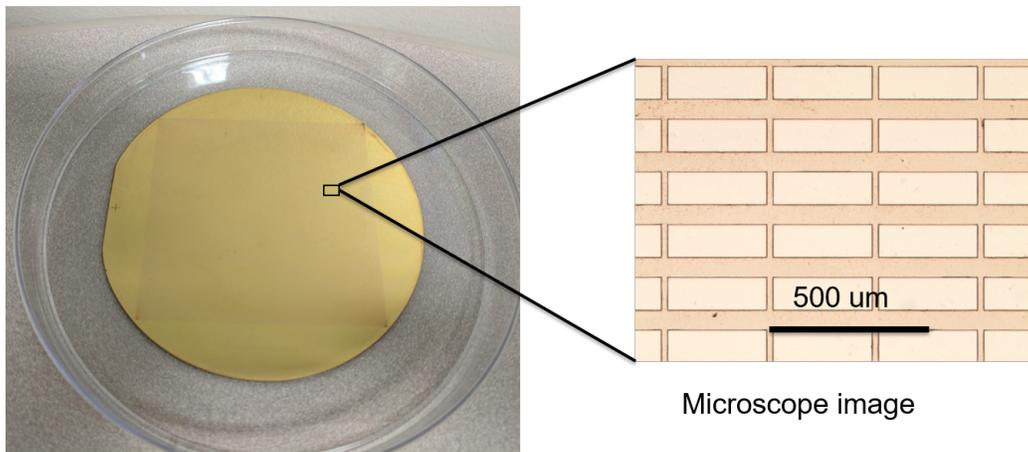


Figure 5. A picture of fabricated metamaterial absorber sample.

An image of the fabricated metamaterial absorber sample is shown in Fig. 5. Due to some over-etching problem, the actual rectangular patch size is around 327 $\mu$m ×106$\mu$m, instead of the designed 340 $\mu$m ×120$\mu$m.

The fabricated sample was characterized in the lab with measurement equipment. The experiment set up is similar to the one shown in Fig. 1. A signal generator connected to an extender module from VDI is used as the source, which is connected to a horn antenna operating at 220-325 GHz. The receiving antenna, which is identical to the transmitting antenna, is connected to another VDI extender, and the frequency is down-converted and detected by a spectrum analyzer. The measurement data is collected and analyzed on a computer. For the measurements, both antennas are placed at an incident angle of 45° to the normal direction of the fabricated sample, and the distance from the tip of the antenna to the surface of the sample is 10 cm.

Fig. 6(a) shows the experiment result of reflection spectrum of the sample between 220 GHz and 320 GHz. The different curves correspond to the rotation angle (in-plane rotation along the axis of the normal direction of the sample surface) of the sample. Similar to simulation results, we see strong resonance when the polarization is aligned with the long side of the rectangular patches (0°). As the sample rotates, the response gets weaker and weaker. When 90° is reached, the spectrum is flat, showing strong reflection similar to a metal plane.
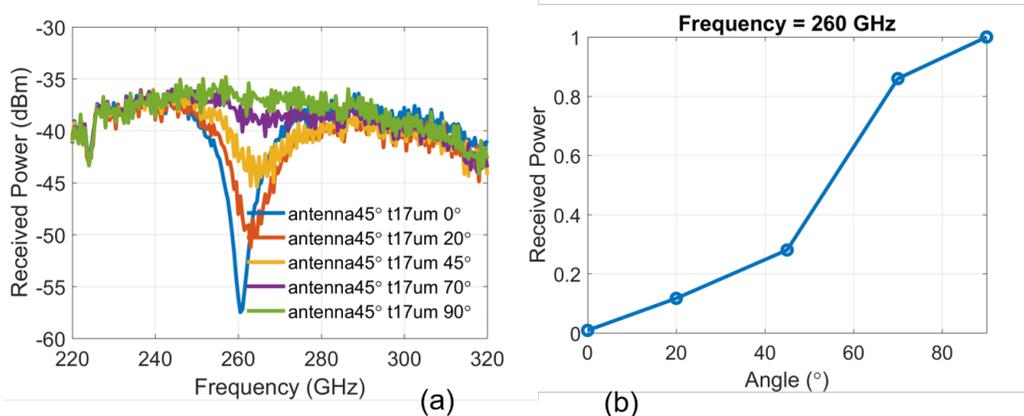
Figure 6. (a) Experimentally measured reflection spectrum for different rotation angles of the metamaterial absorber sample. (b) The reflection as a function of rotation angle at the resonant frequency of 260 GHz.

When operating at the resonant frequency of 260 GHz, we can normalize the measured reflection power to the 90° case. As we can see from Fig. 6(b), the normalized power changes from close to 0 to 1 when the sample is rotated from 0° to 90°.

We also notice a discrepancy in the resonant frequency between the simulation and experiment results. This is due to main two factors: first, as we discussed earlier, during the fabrication process, the feature size is smaller than designed due to over etching; second, there can be a difference in the material parameters, in particular, the parylene properties, between simulation model and the actual values. The discrepancy is not difficult to be compensated in future fabrications.

## 4. CONCLUSIONS

In summary, we presented a THz system with polarization based linear encoder for position sensing. One key component in the system is a barcode that has distinct response between the two linear polarizations. We proposed the use of polarization-dependent metamaterial absorbers to build the THz barcode. We showed with numerical design and initial fabrications and experiments that the metamaterial absorber has distinct contrast of around 20 dB in reflected power between the two polarizations. When switching between the two polarizations, the reflected power changes gradually with the rotation angle. The initial work shows promising results to use the metamaterial absorber as building blocks for a barcode that is polarization-dependent. Future work would include the fabrication of a linear barcode with metamaterial absorbers, and the integration of a THz transceiver to complete the sensing system.

## REFERENCES

[1] Federici, J. F., Schulkin, B., Huang, F., Gary, D., Barat, R., Oliveira, F., and Zimdars, D., "Thz imaging and sensing for security applicationsexplosives, weapons and drugs," *Semiconductor Science and Technology* **20**(7), S266 (2005).

[2] Tonouchi, M., "Cutting-edge terahertz technology," *Nature Photonics* **1**, 97 EP – (Feb 2007). Review Article.

[3] Jepsen, P., Cooke, D., and Koch, M., "Terahertz spectroscopy and imaging modern techniques and applications," *Laser & Photonics Reviews* **5**(1), 124–166 (2011).

[4] Gowen, A., OSullivan, C., and ODonnell, C., "Terahertz time domain spectroscopy and imaging: Emerging techniques for food process monitoring and quality control," *Trends in Food Science & Technology* **25**(1), 40 – 46 (2012).

[5] Ahi, K., Shahbazmohamadi, S., and Asadizanjani, N., "Quality control and authentication of packaged integrated circuits using enhanced-spatial-resolution terahertz time-domain spectroscopy and imaging," *Optics and Lasers in Engineering* (2017).

[6] Nyce, D., [*Linear Position Sensors: Theory and Application*], Wiley InterScience electronic collection, Wiley (2004).

[7] Bigourd, D., Cuisset, A., Hindle, F., Matton, S., Fertein, E., Bocquet, R., and Mouret, G., "Detection and quantification of multiple molecular species in mainstream cigarette smoke by continuous-wave terahertz spectroscopy," *Opt. Lett.* **31**, 2356–2358 (Aug 2006).

[8] Shimizu, N., Ikari, T., Kikuchi, K., Matsuyama, K., Wakatsuki, A., Kohjiro, S., and Fukasawa, R., "Remote gas sensing in full-scale fire with sub-terahertz waves," in [*2011 IEEE MTT-S International Microwave Symposium*], 1–4 (June 2011).

[9] van der Valk, N. C., van der Marel, W. A., and Planken, P. C., "Terahertz polarization imaging," *Opt. Lett.* **30**, 2802–2804 (Oct 2005).

[10] Landy, N. I., Sajuyigbe, S., Mock, J. J., Smith, D. R., and Padilla, W. J., "Perfect metamaterial absorber," *Phys. Rev. Lett.* **100**, 207402 (May 2008).

[11] Tao, H., Bingham, C. M., Strikwerda, A. C., Pilon, D., Shrekenhamer, D., Landy, N. I., Fan, K., Zhang, X., Padilla, W. J., and Averitt, R. D., "Highly flexible wide angle of incidence terahertz metamaterial absorber: Design, fabrication, and characterization," *Phys. Rev. B* **78**, 241103 (Dec 2008).

[12] Tao, H., Landy, N. I., Bingham, C. M., Zhang, X., Averitt, R. D., and Padilla, W. J., "A metamaterial absorber for the terahertz regime: Design, fabrication and characterization," *Opt. Express* **16**, 7181–7188 (May 2008).

[13] Watts, C. M., Liu, X., and Padilla, W. J., "Metamaterial electromagnetic wave absorbers," *Advanced Materials* **24**(23), OP98–OP120 (2012).

[14] Costa, F., Genovesi, S., Monorchio, A., and Manara, G., "A circuit-based model for the interpretation of perfect metamaterial absorbers," *IEEE Transactions on Antennas and Propagation* **61**, 1201–1209 (March 2013).

[15] Sellier, A., Teperik, T. V., and de Lustrac, A., "Resonant circuit model for efficient metamaterial absorber," *Opt. Express* **21**, A997–A1006 (Nov 2013).

[16] Chen, H.-T., "Interference theory of metamaterial perfect absorbers," *Opt. Express* **20**, 7165–7172 (Mar 2012).

[17] Liu, X., MacNaughton, S., Shrekenhamer, D. B., Tao, H., Selvarasah, S., Totachawattana, A., Averitt, R. D., Dokmeci, M. R., Sonkusale, S., and Padilla, W. J., "Metamaterials on parylene thin film substrates: Design, fabrication, and characterization at terahertz frequency," *Applied Physics Letters* **96**(1), 011906 (2010).